arXiv:1512.01620v2 [astro-ph.GA] 13 Feb 2016

Modeling GD-1 Gaps in a Milky-Way Potential

R. G. Carlberg

Department of Astronomy & Astrophysics, University of Toronto, Toronto, ON M5S 3H4, Canada

carlberg@astro.utoronto.ca

ABSTRACT

The GD-1 star stream is currently the best available for identifying density fluctuations, "gaps", along its length as a test of the LCDM prediction of large numbers of dark matter sub-halos orbiting in the halo. Density variations of some form are present, since the variance of the density along the stream is three times that expected from the empirically estimated variation in the filtered mean star counts. The density variations are characterized with filters that approximate the shape of sub-halo gravitationally induced stream gaps. The filters locate gaps and measures their amplitude, leading to a measurement of the distribution of gap widths. To gain understanding of the factors influencing the gap width distribution, a suite of collisionless n-body simulations for a GD-1 like orbit in a Milky Way-like potential provides a dynamically realistic statistical prediction of the gap distribution. The simulations show that every location in the stream has been disturbed to some degree by a sub-halo. The small gaps found via the filtering are largely noise. Larger gaps, those longer than 1 kpc, or 10° for GD-1, are the source of the excess variance. The suite of stream simulations shows that sub-halos at the predicted inner halo abundance or possibly somewhat higher can produce the required large sale density variations.

Subject headings: dark matter; Local Group; galaxies: dwarf

1. INTRODUCTION

The GD-1 star stream (Grillmair & Dionatos 2006) is, at 70 pc width, one of the thinnest known. The implied low velocity dispersion, about 1 $\mathrm{km\,s^{-1}}$, means that GD-1 will respond coherently to the passage of the many low mass dark matter sub-halos predicted to present in the galactic dark matter halo in an LCDM cosmology (Springel et al. 2008; Diemand, Kuhlen & Madau 2007; Stadel et al. 2009). A dark matter sub-halo passing very near of through

the streams causes a folding (Carlberg 2009) which observationally appears as density peaks on either side of a low density gap (Yoon, Johnston & Hogg 2011; Carlberg 2012; Erkal & Belokurov 2015). Assuming an LCDM cosmology allows concrete, statistical, predictions of the properties of the induced irregularities in star streams which can be compared to observational data. There are alternatives to LCDM cosmology which work well on galactic scales and do not predict large numbers of unseen dark matter sub-halos (Kroupa 2015).

GD-1 is visible over about 80° of high latitude sky where extinction is low. Since the visible section of the stream is a relatively nearby 8 kpc, SDSS (York et al. 2000) imaging data reach the turn-off stars where the luminosity function rises steeply. Grillmair & Dionatos (2006) estimated 1800±200 stars were visible in the 63° of stream they examined. Radial velocities (Yanny et al. 2009) and mean proper motions (Munn et al. 2004, 2008), provide some stream averaged phase space information (Willett et al. 2009; Koposov et al. 2010) along the stream. The derived orbits have a perigalacticon of about 14 kpc and apogalacticons of 26-29 kpc. No progenitor for the GD-1 stream has yet been identified close to the orbit of the stream, although the very low velocity dispersion of the stream strongly suggests that the progenitor is (or was) a low mass globular cluster.

Carlberg & Grillmair (2013) characterized the gaps within GD-1 using a set of gap shaped filters that are convolved with the density along the stream. The outcome is the identification of the locations and sizes of gaps. The result for GD-1 was a distribution of gap sizes that behaved about as the predicted power law for gaps larger than 2° (using a width defined with the negative part of the gap) and flattened off for smaller gaps. The paper noted that the internal velocity dispersion and shear in the stream suppressed small gaps below the numbers predicted from a cold stream model, which was quantified to some degree in Carlberg (2015a).

The purpose of this paper is to compare the distribution of gap sizes in GD-1 to the same measurements of dynamically realistic models of the GD-1 stream. The stream progenitor will be assumed to be a low density globular cluster on a GD-1 like orbit in a potential that approximates the Milky Way and contains the predicted level of dark matter sub-halos. A set of simulations is undertaken since the gaps in any one stream depend significantly on the random variations in the sub-halo population as realized from the same parent population of sub-halos. The resulting streams are projected onto the sky and analyzed with the gap filtering technique, which is applied in exactly the same way to the observational data. The goal is to quantitatively understand the numbers of GD-1 detected gaps as a function of their size as a test for consistency with the LCDM sub-halo predictions.

2. Gaps in The GD-1 Stream

The density of stars along the GD-1 stream was measured (Carlberg & Grillmair 2013) using the SDSS DR-8 photometric data (Aihara et al. 2011). Their filtered density of stars along the stream, rebinned to 2° intervals, is shown in Figure 1. Foreground and background stars along the line of sight to GD-1 are greatly, but far from completely, suppressed with a matched filter designed to pick out old metal poor stars in stellar color-magnitude data (Rockosi et al. 2002; Grillmair 2009, 2011). The mean over-density of the filtered stream is 14% above the filtered mean background density.

The errors in the stream density measurement is estimated from the variance in the field star density near to the stream., augmented with the slight extra noise that the mean stream itself will contribute. The resulting signal-to-noise ratio per 2° bin is 2.3. However, the variance in the stream density is more than three times what is expected for a unstructured, but noisy, stream and is strong statistical evidence that the stream contains some form of excess density variations.

To characterize the excess variance of the stream density, we use a gap-filter designed to approximate the shapes of stream gaps (Carlberg 2013). The filters have a negative density in the center with two positive density peaks on either side. The filters have zero mean over the range $x = [-3, 3]$ and are normalized to unit variance. Our preferred filter is $w_1(x) = (x^6 - 1)\exp(-1.2321x^2)$ but as an alternate we use the spikier $w_2(x) = (x^8 - 1)\exp(-0.559x^4)$, although a continuum of filter shapes should be examined at some future step. As a first step towards recognizing that gaps are generally not symmetric (Sanders et al. 2015), we introduce some asymmetry with a simple linear function, $a(x) = 1 + \alpha x$, to create a right enhanced asymmetric filter version of the w_i filter, $w_{ir}(x) = w_i(x)a(x), x > 0$ and $w_{il}(x)/a(x), x < 0$, with its left enhanced partner being the reversed version. We use $\alpha = 0.25$, however a whole continuum of α values could be examined. To prepare the density field for filtering, it is normalized to a mean of unity, which is then subtracted. We then pass the densities through a Gaussian high pass filter having a filter scale of half of the fundamental wavelength of 73°.

Gap filtering transforms the one dimensional stream densities as a function of angular distance along the stream, $d(\phi)$, into a two dimensional space of stream position and filter width, $D(\phi, g)$. The filter argument, x is $x = \phi/g$ where g begins at the bin size. The value of g goes to 50° (which is larger than the maximum allowed gap in GD-1) in 100 logarithmic steps per decade, which creates 393 filters in total. Finer steps in filter size make no difference to the outcome and even ten times coarser steps lead to relatively small differences in outcome. Peaks in this two dimensional space are identified as points higher than the neighboring points, here simply the neighboring two points in x and two in the

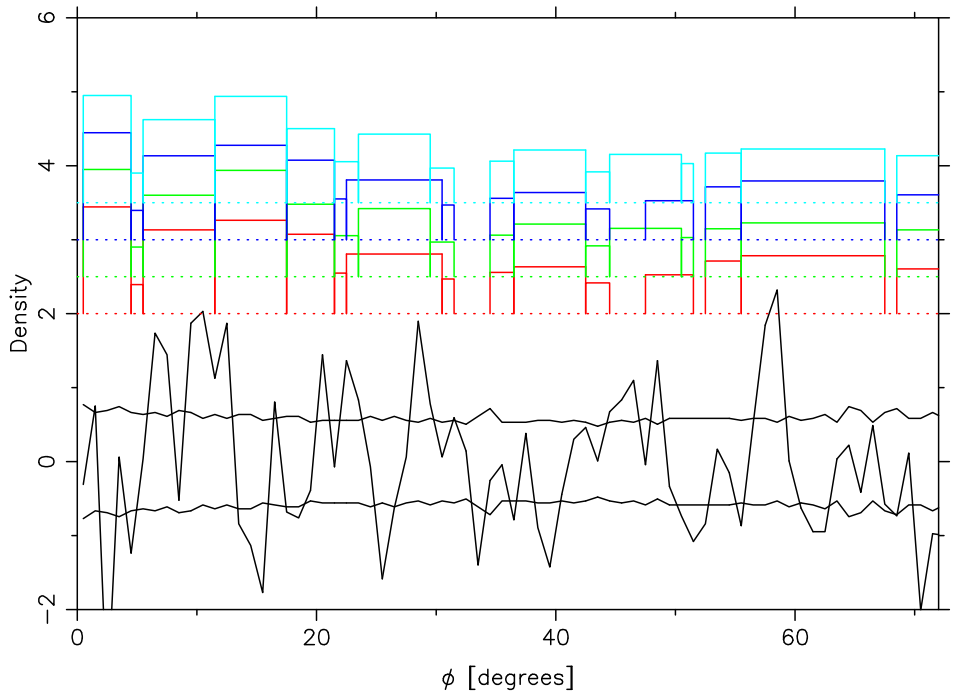


Fig. 1.— The density along the GD-1 stream (jagged line) from the measurements of Carlberg & Grillmair (2013) re-binned to 2° and normalized to a mean of one which is then subtracted. The accompanying pair of lines show the locally estimated $\pm 1\sigma$ standard deviation of the density. The histograms are the gaps recovered from this stream data in the gap-finding procedure discussed in the text. The gaps here include the compensating high densities on either side so the gaps here are defined to be three times the width used in Carlberg & Grillmair (2013). Starting from the bottom, the histograms are the results for the w_1 (red) and w_2 (green) symmetric filters, and then the same filters augmented with their asymmetric versions, blue and turquoise, respectively.

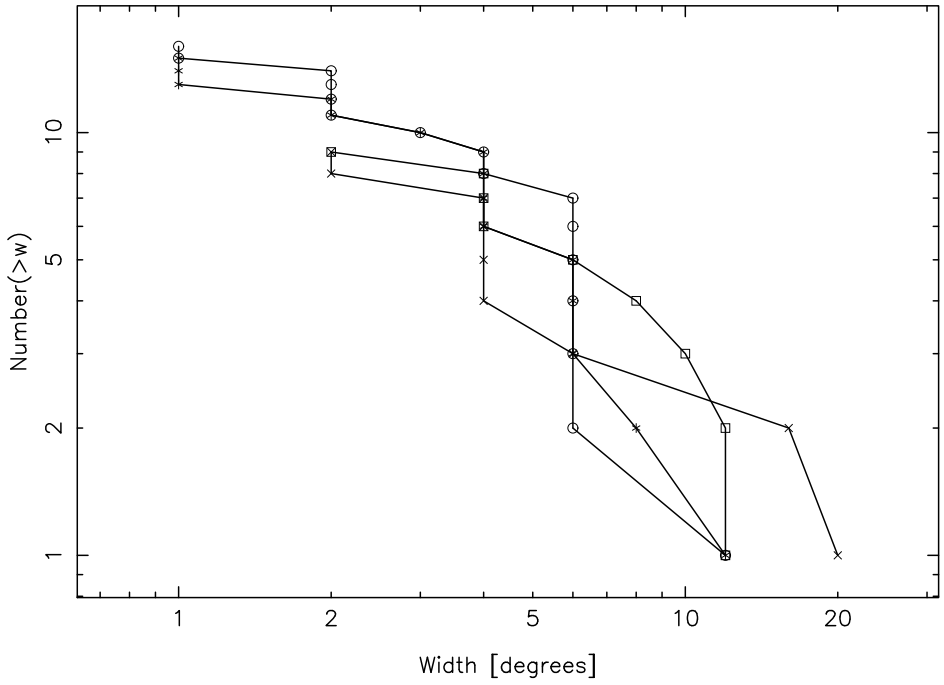


Fig. 2.— The cumulative number of gaps as a function of their width and filter shape used. The symbols are, for 1 degree bins: asterisk, circle, and for 2 degree bins: cross, square, where the first and second member of each pair is filter 1 and 2, respectively.

values of g (where g may include asymmetric filters as well). At any given ϕ value there are likely to be peaks at a number of differing g values. The height of the peak depends on how well matched the shape of the filter is to the density profile at that location in the stream. A perfect match with no noise would give a peak height of one. Each filter is normalized to allow the comparison of filters of different sizes. To place density bins into a unique gap (or no gap at all) we start at the gaps found for the smallest g value which identifies a series of peaks along the stream. The points within width $\pm$3g of each peak that is above some minimum threshold height into a gap. We then examine the next g value upward in size. Any peaks of a longer filter that are higher than for a lower filter takes over the bins within a shorter filter gap. This procedure is continued to the largest g value and leads to bins being placed into gaps of varying widths and heights. A very low threshold for allowing a gap means that virtually the entire density field is in gaps with a very high threshold requiring an extremely good match to the prescribed shape of the gap. We will turn to stream simulations for guidance on how to interpret the gaps.

Figure 1 displays the results of the gap filtering applied to the GD-1 densities in 2° bins. The gaps are defined as initially extending over [-3g, 3g] not allowing any of the included region to have a gap unless it is a deeper gap. Longer gaps can take over some or all of a shorter gap. In detail these procedures are similar but not identical to those used in Carlberg & Grillmair (2013). The gaps in Carlberg & Grillmair (2013) were defined to initially extend from [-g, g], roughly the negative density region of the gap and 1/3 of the widths adopted here. The gaps resulting from the revised analysis here are displayed with a vertical offset of 0.5 units at the top of the density plot, Figure 1. The w_1 (red) and w_2 (green) filters largely lead to similar results. The same filters augmented with their left and right asymmetric versions, blue and turquoise, respectively, again give very similar results, with one notable large gap being preferred over several smaller gaps for the asymmetry allowed w_2 (turquoise, the top set of gaps).

Figure 2 shows the cumulative number of gaps greater in length than some value w, $N(>$ w) for the two symmetric filters, here run on the density field binned into both 1° and 2° bins. Overall the two filters and the two different data bin widths recover a similar underlying distribution of widths. However, the 1° binning has a large number of small gaps recovered. The excess of small gaps in the 1° binned data over those in the 2° binned data is nearly a factor of 3 and it is reasonable to suspect the increased numbers of gaps at small scales is largely due to noise.

3. GD-1 Stream Simulations

Carlberg & Grillmair (2013) compared similar, but not identical, gap measurements of GD-1 to predictions from approximate fits to a set of simulations of streams in a external potential with orbiting sub-halos derived from the Springel et al. (2008) LCDM numerical model halo. A limitation of that work is that the theoretical analysis examined only streams on circular orbits, where gaps are much simpler and persist long than a stream on an elliptical orbit. The sub-halo interactions with the stream were done individually with the cumulative effect simply being the mass weighted sum over all sub-halos, with no allowance for overlap (Ngan & Carlberg 2014).

Simulations are essential to give the appropriate range of ages along the stream, the gap-blurring of velocity dispersion and velocity shear across the stream, and the internal structure of the stream which varies with orbital phase. The dynamical properties of the leading and trailing streams drawn out of a globular star cluster progenitor through tidal heating can be accurately calculated within a collisionless n-body code (Carlberg 2015a; Sanders et al. 2015). Allowing two-body relaxation between stars within the cluster (Küpper et al. 2010, 2012) adds more precision for the stream properties of those clusters where energy equipartition processes are important, but requires a more detailed description of the cluster and its contents and adds computational costs.

The Milky Way potential MWPotential2014 (Bovy 2015), here referred to as MW2014, is a somewhat simplified (it has no bar, for instance), easy-to-use, potential designed to provide a good description of the mean axisymmetric Milky Way potential from well inside the solar circle to 60 kpc, which more than covers the radial range that the orbit of GD-1 traverses. The assumption of an axisymmetric potential eliminates most chaotic orbit possibilities (Price-Whelan et al. 2015). The MW2014 dark halo component is described with an NFW model function (Navarro et al. 1997). The scale radius of 16 kpc, very similar to the value of $r_{200}/c_{NFW} = 15.3$ kpc of the Aquarius numerical model (Springel et al. 2008). MW2014 has an enclosed dark matter mass out to 245 kpc of $8.1 \times 10^{11}\,\mathrm{M}_\odot$, 44% of the Aquarius mass to that radius, which proportionally reduces the total mass of sub-halos.

The model contains a set of sub-halos which interact with the stream to create gaps in a realistic manner. Over a galactic lifetime the gaps can overlap, which is naturally taken into account. The sub-halos are much less concentrated than the dark matter, with a radial distribution well described with an Einasto function (Springel et al. 2008) where we use their overall fractional mass normalization, although the total dark halo here is less massive than in their simulations. The local mass fraction in sub-halos inside 16 kpc is 0.0014 with a fraction of 0.0038 inside 32 kpc, that is, sub-halos are are very small fraction of the mass in the inner halo. Out to 245 kpc, the r_{200} radius of Aquarius, the mass fraction in sub-halos

rises to 0.058.

The sub-halo distribution is assumed to be spherical, as is the overall dark matter halo. The Milky Way sub-halos surrounding dwarf galaxies are known to be in a fairly flattened distribution (Lynden-Bell 1976; Pawlowski et al. 2012; Pawlowski & Kroupa 2014) with the distribution of the unseen sub-halos of course not known. If they have the same distribution as the visible ones then the rate of interactions will depend on the orbit of GD-1 relative to the plane of satellites. Willett et al. (2009) find that the GD-1 orbit is inclined to the galactic plane about 35°, so the pole of the orbital plane is 55° from the galactic plane, currently in a direction away from the galactic center, but the orbit precesses slowly around the galactic pole. Pawlowski & Kroupa (2014) find a satellite plane pole at $\ell \simeq 159°$, $b \simeq -5$ and that the average distance from the pole to all satellite orbit poles is 48°. Therefore this crudely estimated GD-1 orbital pole lies within that angular distance, but near the outer edge of the cluster of points shown in their Figure 3. Modeling the plane of satellites as flattened sphere finds a $c/a \simeq 0.25$ for a sample including lower mass dwarf galaxies (Pawlowski 2016). Therefore the interactions would enhanced up to a factor of four if the stream lay exactly in the plane and less with increasing misalignment. This is a potentially interesting effect which merits further investigation.

The GD-1 stream has an inferred orbital pericenter of approximately 14 and apocenter of 30 kpc. To fully populate our model with sub-halos that have pericenters outside this range would be computationally inefficient. The radial distribution of sub-halos is smoothly diminished to zero at large radius with the function $\exp\left[-\frac{1}{2}(r/r_g)^3\right]$. Recalling that the inferred apocenter for GD-1 is a little under 30 kpc, r_g is set at 7 scale radii, or 56 kpc, which leaves the inner region largely intact except for sub-halos on very low probability very radial orbits, but fairly quickly reduces the numbers at larger radii. The outcome is that within 245 kpc the sub-halo numbers are reduced 91% with only a 4% reduction inside 32 kpc. Sub-halos are randomly drawn from the resulting radial distribution and placed in a random spherical distribution. The equilibrium velocity dispersion of this distribution is calculated from Jeans' equation using the spherical halo alone. We then have radial density and velocity distribution function which we use to set up the population of sub-halos in an approximate equilibrium. Although the calculation ignores the bulge and disk components of the inner potential the distribution is sufficiently close to equilibrium for our purposes in the region of the GD-1 orbit, see Figure 3, where the initial and final sub-halo distributions are visibly similar.

The mass distribution of sub-halos is generated from the Springel et al. (2008) number-mass distribution, $N(>m) \propto m^{-0.9}$. The masses are restricted to a maximum where they would have a short dynamical friction time, and, a minimum below which their effects on

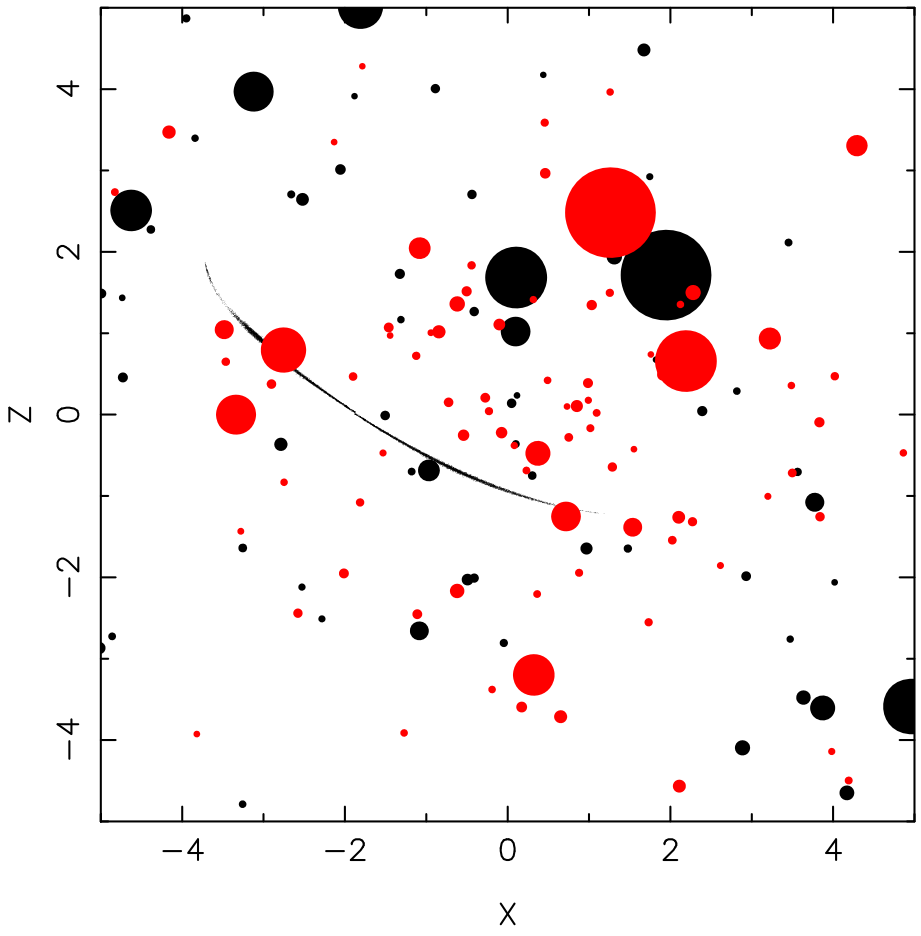


Fig. 3.— The edge-on projection of the distribution of sub-halos at the beginning (black) and end of a simulation, 10.44 Gyr later (red), with the stream shown at the end of the simulation. The sub-halos are given a size 5 times their scale radius. A density weighted version of the stream would appear thinner. One unit of distance is 8 kpc. The solar location is in the galactic plane, $z = 0$, at $x = 1$.

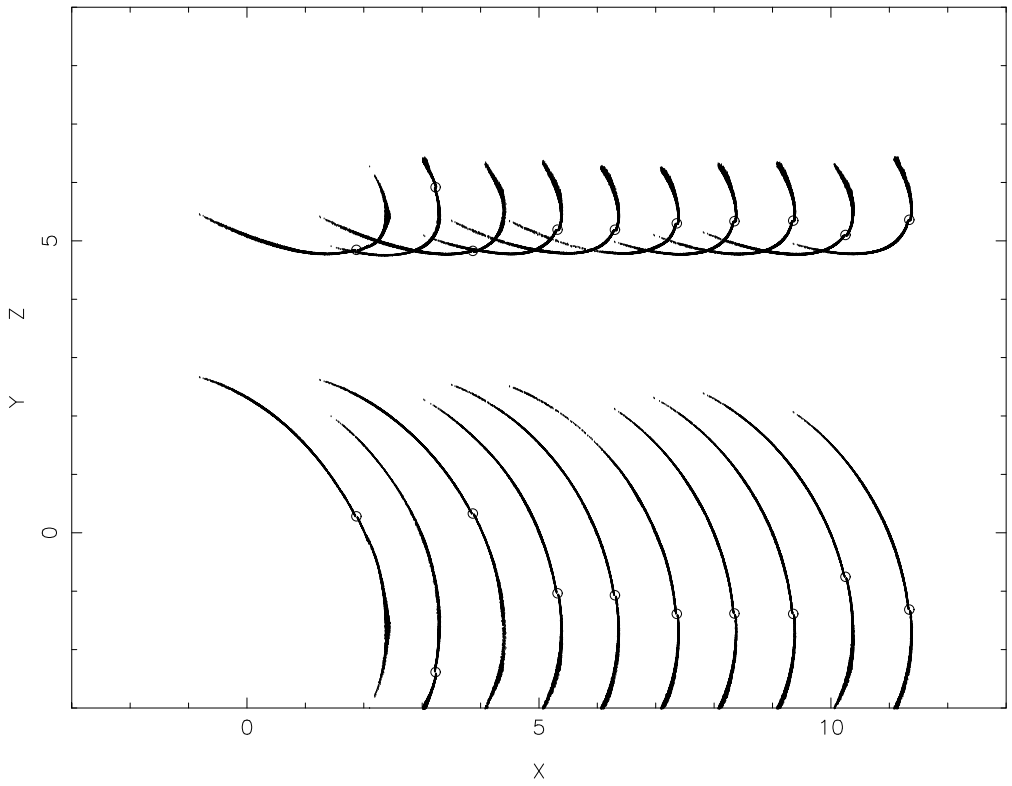


Fig. 4.— xy (lower row) and xz (upper row) plots for ten realizations of the same initial conditions. The streams are all viewed at the same time, 293.6, 10.44 Gyr from the start, offset 1.0 in x with each plot. The progenitor centers, marked by the circles, vary because the sub-halos induce small changes in its orbital period.

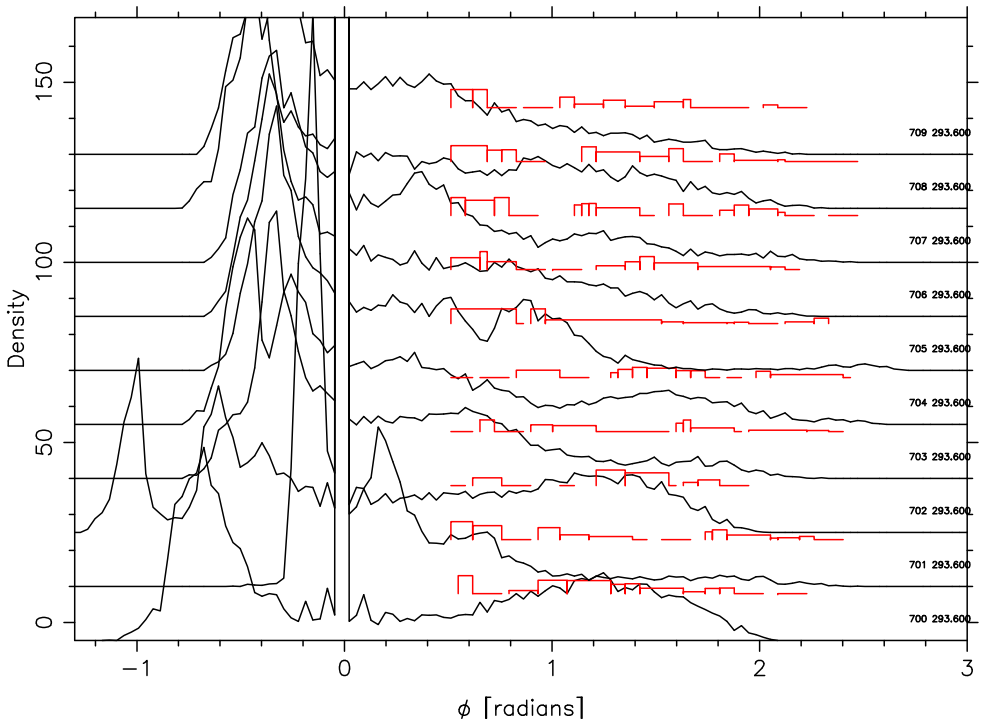


Fig. 5.— The density along the stream for the ten realizations of the eccentricity 0.32 stream at 10.44 Gyr age, the same time as shown in Figure 4. Angles are measured with respect to the progenitor which defines an angle of zero and has the large density peak. The midpoint of the leading arm of the stream is near pericenter and near the solar location of $x = 1$, see Figure 4, roughly replicating the GD-1 observations. The stream is observed from a position offset from the center, equivalent to the solar radius in the model. The gap analysis in this figure is allowed to extend over larger angles than used for our GD-1 comparison. The large density peak at negative angles (trailing arm of the streams) is the result of particle pileup at lower angular velocities at large radial distances, and, increased distance from the viewing point. A very massive sub-halo has gone through the trailing arm of the stream second from the bottom. The lowest density line shows the Küpper et al. (2012) epicyclic variations are only visible for about two cycles away from the progenitor.

the stream are negligible. That is, the dimensionless mass range of sub-halos is 3×10^{-3} to 3×10^{-6}, where one mass unit in MW2014 is $9.006 \times 10^{10}\,M_\odot$, or 2.7×10^8 to $2.7 \times 10^5\,M_\odot$. The total sub-halo mass contained to the minimum sub-halo mass allowed is 50% of the total in the mass range down zero mass. These numbers vary from halo to halo and the numbers in the inner halo will vary depending on recent mergers. For the adopted normalization there is typically one sub-halo generated above $m = 10^{-3}$ ($9 \times 10^7\,M_\odot$), with a median total number of about 120 with individual runs in a suite of 100 ranging from about 14 to 219.

The star cluster is usually simulated with 50,000 particles, but some higher resolution results with 500,000 particles are reported below. The system is evolved with the parallel shell code described in Carlberg (2015a) which provides high dynamical accuracy at reasonably low cost. This code is, by design, collisionless and does not capture any of the complex collisional processes that can drive evaporation in dense, low velocity dispersion, globular clusters. There are two reasons that a collisionless cluster is an acceptable approximation for our study. First, for clusters on eccentric orbits the rate of tidal heating occurs on an orbital time scale and generally exceeds the two-body heating of core collapse, an example being the relatively diffuse Pal 5 cluster and its associated stream. Second, GD-1 has no known progenitor to use to determine the importance of two-body relaxation processes.

The MW2014 potential is the external potential in which the sub-halos orbit as test particles. The star cluster is self-gravitating and responds to the sub-halos. The code accurately reproduces the results of a full n-body code for situations of interest. All particles are advanced with time steps of 0.002 units using a leap-frog integrator. The small time steps capture the internal dynamics of the star cluster and the interactions between the stream and sub-halos. The simulations run to time 300, where one time unit in MW2014 is 3.556×10^7 years, so a duration of 10.67 Gyr.

The star cluster is started on an orbit similar to that inferred for GD-1, with no attempt to replicate it precisely. The starting point is $x = 3.6$ (28.8 kpc), $y = 0$, $z = 2.5$ (20 kpc), which is approximately the location of the current orbital apocenter of the stream(Willett et al. 2009; Koposov et al. 2010). The progenitor is started with a purely tangential velocity, $v_x = v_z = 0$, v_y of 0.85 of the local circular velocity calculated from the MW2014 potential. The resulting orbit has an eccentricity of 0.32, essentially equal to the 0.33 inferred for GD-1 (Willett et al. 2009). We also ran orbits with a starting velocity of 0.7 of circular, which leads to an orbital eccentricity of 0.44. A more eccentric orbit has the benefit of increased mass loss, roughly 55% as opposed to the 24% for the lower eccentricity, which provides better statistics in the stream. Although more eccentric orbits will generally blur out gaps more quickly we find that the gap spectrum is very similar for these two fairly similar orbits.

3.1. Stream Realization-to-Realization Variations

The stellar streams that develop in the simulations need to be put into coordinates similar to those for GD-1 to make the gap distributions and the density alone the stream usefully comparable. The density of stars in the stream varies along its length and with time if the progenitor is in an elliptical orbit (Johnston 1998). Viewed from the center of the galaxy the mean density in angular coordinates peaks where the stream is moving slowly and the stream is far from the center, that is, at apocenter, and is low at pericenter. Having a long angular segment at fairly constant density requires a point of observation close to one of these locations, which for GD-1 is pericenter. We therefore analyze times when some portion of the stream is near pericenter and place a point of observation nearby. The nearly constant density profile of GD-1 is largely a remarkable coincidence of timing and location relative to the solar location, and of course it is much easier to find streams nearby.

The position and angular momentum of the progenitor cluster defines an instantaneous orbital plane and a great circle around the sky. The point of observation is at the solar position, 1 unit (=8 kpc) from the model center at a location of [x,y,z] = [0.707,0.707,0], see Figure 4. The stream is observed at time 293.6, or 10.44 Gyr, the time for the streams shown in Figure 4. The stream particle positions are projected onto the coordinate system for each simulation and assigned angles relative to the progenitor center. At this time and position the leading arm of the stream appears to have an angular distance on the sky of nearly 180°. If observed from the center the stream would be shorter and the density distribution would have a larger mean density variation along the stream. All of the results and plots here are measured in the coordinates of the solar position analog.

The densities along the stream for ten realizations of the standard initial conditions are shown in Figure 5, observed from the solar position analog. The primary difference between the simulations is the distribution of sub-halos. In particular the heaviest dozen or so sub-halos have the largest effects and can have very different orbits that may or may not lead to any intersections with the stream. The variation from realization to realization is substantial. Consequently the prediction of the number and width of gaps along the stream will be a statistical prediction.

3.2. Sub-halo Mass Subsets and Stream Variations

The effect of different mass ranges of sub-halos is displayed in Figure 6 for one of the standard stream simulations. The line at the bottom of the plot is the density along the leading arm of the stream for the 101 sub-halos over the whole mass range from 3×10^{-3} to

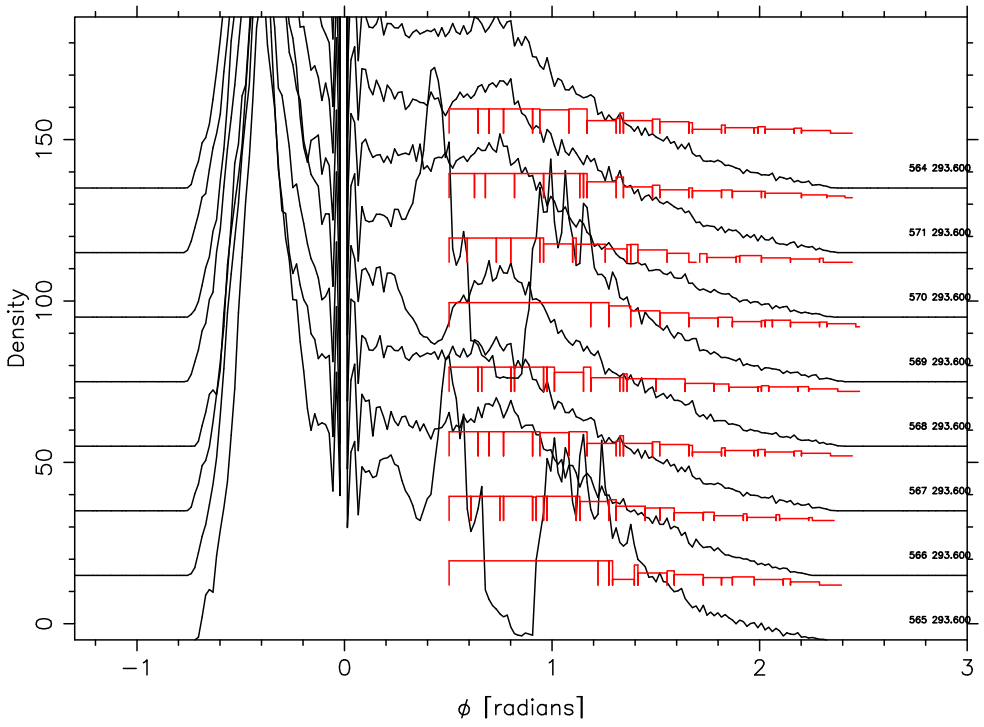


Fig. 6.— A stream with a 500,000 particle progenitor displayed with all sub-halos (bottom) and then rerun with sub-halos in successively smaller mass ranges (see text), with the top density distribution being for a reference model with no sub-halos. The mass ranges span a factor of 1000 in mass with approximately equal mass in each range. In this case the large gap is the result of the 7 mid-mass range sub-halos, not a single large sub-halo.

3×10^{-6}. (2.7×10^8 to $2.7 \times 10^5\,M_\odot$). Second from the bottom is the mass range 3×10^{-3} to 1×10^{-3} (2.7×10^8 to $9 \times 10^7\,M_\odot$), in which there is one sub-halo. Typically there is a single halo is present in this mass range and it hits the stream about half the time. In the mass range 1×10^{-3} to 3×10^{-4} (9×10^7 to $2.7 \times 10^7\,M_\odot$) there are no sub-halos, 3×10^{-4} to 1×10^{-4} (2.7×10^7 to $9 \times 10^6\,M_\odot$) has 4, 1×10^{-4} to 3×10^{-5} (9×10^6 to $2.7 \times 10^6\,M_\odot$) has 7, 3×10^{-5} to 1×10^{-5} (2.7×10^6 to $9 \times 10^5\,M_\odot$) has 27, and at the top 1×10^{-5} to 3×10^{-6} (9×10^5 to $2.7 \times 10^5\,M_\odot$) has 62. These numbers are for the restricted inner halo sub-halo population, but do reflect that for the MW2014 potential's dark matter sub-halo the numbers of dynamically relevant sub-halos are not large. The simulations show how the overlap of sub-halo impacts on the stellar stream makes individual sub-halo hits very difficult to discern unless the sub-halo is very massive. Even then, smaller mass sub-halos, those near $m = 10^{-4}$, or $10^7\,M_\odot$, can create significant structure on the density profile as is dramatically shown in Figure 6, where the 7 halos that are individually about 3% of the maximum allowed mass, create a gap that could be mistaken for the passage of a single much more massive halo.

Smaller mass sub-halos, those below 1×10^{-5}, or $10^6\,M_\odot$, second and third from the top in Figure 6, produce projected density variations so small that they are barely distinguishable from the no sub-halo case, the top line in Figure 6. Figure 6 shows that the combined effect of sub-halos is not a simple sum in density space of the outcomes of individual sub-halos. That is the density (and velocity) fluctuations in a stream as a result of population of sub-halos is substantially non-linear, even though the changes in orbital momentum variables (actions) of individual particles remain effectively in the linear regime. As a consequence it will be very difficult, if not impossible, to infer the properties of individual lower mass sub-halos even with full phase space information for the stars in the stream. Massive sub-halos, those up around $10^8\,M_\odot$ (10^{-3} in our dimensionless units) are relatively rare and cause large perturbations in a stream so offer an opportunity for individual study although even their gaps are perturbed by the lower mass sub-halos that are present.

4. Gaps in GD-1 like simulations

One hundred realizations of clusters on the GD-1 like orbit in the MW2014 potential are run for 300 time units, or 10.67 Gyr . We focus on time 293.6, 10.44 Gyr, which is the last orbit when the leading arm of the stream is in a configuration somewhat similar to GD-1, where the stream is near pericenter and near the sun.

Küpper et al. (2008, 2012) demonstrate that as the gravitational tide of the host galaxy pulls stars away from a globular cluster that coherent epicyclic orbital motions of the stars

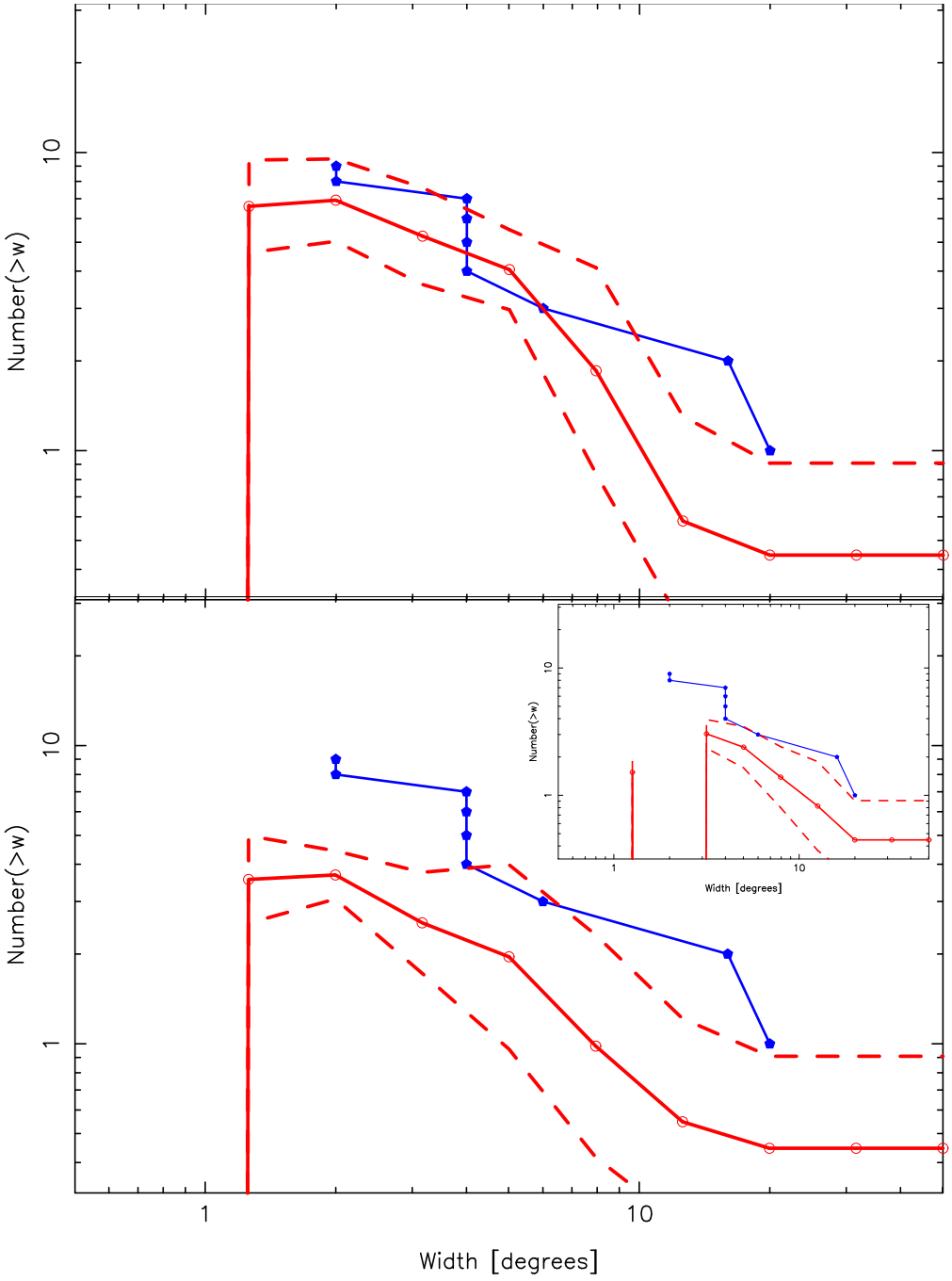


Fig. 7.— The gap distribution found with the w_1 filter averaged over 100 simulated streams at time 293.6, 10.44 Gyr, at full resolution with the RMS deviation from the mean plotted above and below the mean as dashed lines. The same filter applied to GD-1 is shown as (blue) line with points. The minimum gap height is 0.01 in the top panel and 0.1 in the bottom panel. The inset figure in the lower panel shows the same analysis at time 154, 5.48 Gyr, requiring a minimum gap height of 0.1.

leads to density variations in the tidal stream. These density variations naturally appear in the simulations here as well but are only important near the progenitor system as is visible in Figure 5. We do not want to confuse these variations with sub-halo density variations, so the measurements of our simulations exclude the region near the progenitor, specifically the 40° of the stream closest to the progenitor. Recall that GD-1 has no visible progenitor, so this exclusion region is appropriate.

The offset viewing point near pericenter leads to densities along the stream are relatively constant with azimuthal angle, similar to GD-1. The particles are placed into density bins the same size as used in the GD-1 analysis, usually 2°. The resulting density along the stream is passed through a Gaussian high pass filter that removes the large scale density variations of the stream so that the emphasis is on the gaps, not the large scale density variations.

The number of gaps depends on the minimum height threshold used. A minimum height of 0.1 gives all the gaps of the real GD-1. A "perfect" noiseless gap that exactly matches the filter shape and has a depth such that the density goes to zero at the bottom would give a gap of height of exactly 1.0. We use gap height thresholds of 0.1, which selects the more robust features of the simulations and includes all of the GD-1 gaps that the algorithm finds, and a low threshold of 0.01, which usually finds all the gaps to be found in the simulations.

4.1. Gaps in Low Noise Streams

First we examine simulated streams with about a factor of 3 to 4 higher signal to noise in the currently available GD-1 data. In Figure 7 in the top panel the minimum gap height allowed is 0.01 which collects all the gaps in the simulations at time 293.6, 10.44 Gyr. The displayed quantities are the mean and the 1σ confidence interval which are calculated from the standard deviation of the counts. Also shown in Figure 7 is the GD-1 gap distribution measured with precisely the same parameters. The numbers of small separation gaps increase significantly as the minimum gap height counted decreases, indicating that noise is a major factor for their numbers. The numbers of large gaps in the simulations are not very sensitive to the minimum gap height. Moreover, there is generally good agreement with the GD-1 measurements of larger gaps.

The number of gaps depends on the minimum gap height allowed for counting. The lower panel of Figure 7 shows the gap distribution with a minimum height counted of 0.01, showing that most of the small gaps are relatively small amplitude gaps but that the bigger gaps are relatively high amplitude. A set of these gap size distributions for a subset of ten simulations is shown in from Figure 5. The inset in the lower panel of Figure 7 shows the

mean gap distribution at time 154, 5.48 Gyr, about half the age of the other plots, for the 0.1 minimum gap height. The large gaps are, on the average, already at the mean level seen at the end of the simulations, although the spread of values about the mean is somewhat smaller. That is, the gap distribution becomes stable at about half the Hubble age, when sufficient stream length is available and as new gaps are created older ones fade away. This is expected since the lifetime of smaller gaps in a stream with a GD-1 like orbit is typically 5 to 6 orbits, or about 3 Gyr, (Carlberg 2015a).

We also explore the outcome with the mass fraction in sub-halos increased. Doubling the mass fraction in sub-halos doubles the number of large sub-halos intersecting the streams, but they remain sufficiently infrequent that the overall distribution remains about the same. For an extreme effect, the mass in sub-halos is increased a full factor of 10 which boosts the active sub-halo mass fraction in the inner region to 1.9% from 0.19% so the simulation remains physically sensible, although perhaps cosmologically implausible except during major accretion events. In this case there are so many large sub-halo hits that the stream always displays large deep gaps with a range of density contrast about 3 times larger than those seen in the simulations with the standard parameters. These large density variations do not appear to exist in the GD-1 data. The extreme density structures shown in Figure 8 are not very successfully recovered with the current gap filters.

4.2. Gaps in Noisy Streams

Figure 9 shows the gap spectrum for essentially pure noise, created by adding a Gaussian random number to the stream densities sampled at the rate of one particle out of one hundred. In addition to the mean and 1σ spread, the circles show the result of the individual measurements of the 100 streams. The noise explains all the gaps smaller than about 8°, but falls short of the gaps greater than 10°. It is also notable that the pure noise gap distribution has a much smaller spread of distributions around the mean compared to the stream results. Quantitatively, gaps of 10° and larger are less than 1% probable from noise. That is, at 99% confidence the large gaps are not due to noise alone. We now can claim to understand the nature of the excess variance in the GD-1 stream: it is due to an excess of density variations that match the shape of gaps over scales of 10° and larger.

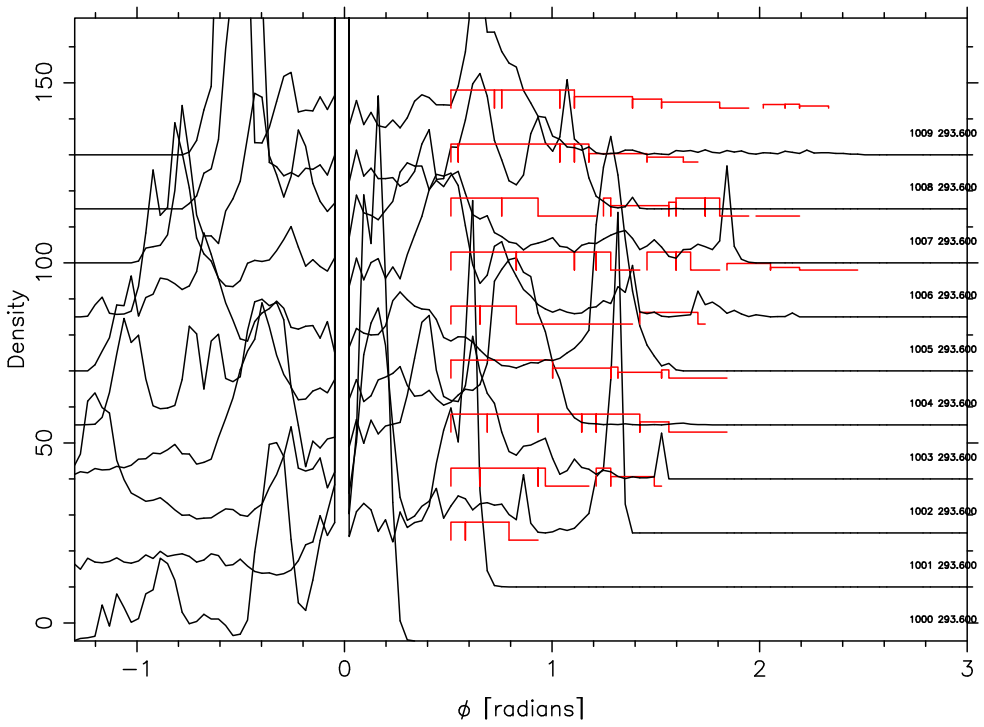


Fig. 8.— Same as Figure 5 except for a sub-halo mass fraction raised a factor of ten, leading to ten times the number of sub-halos. The vertical scale has been kept the same as the earlier figure to emphasize the how extreme the density variations are. The angular phase differences between simulations are also much larger.

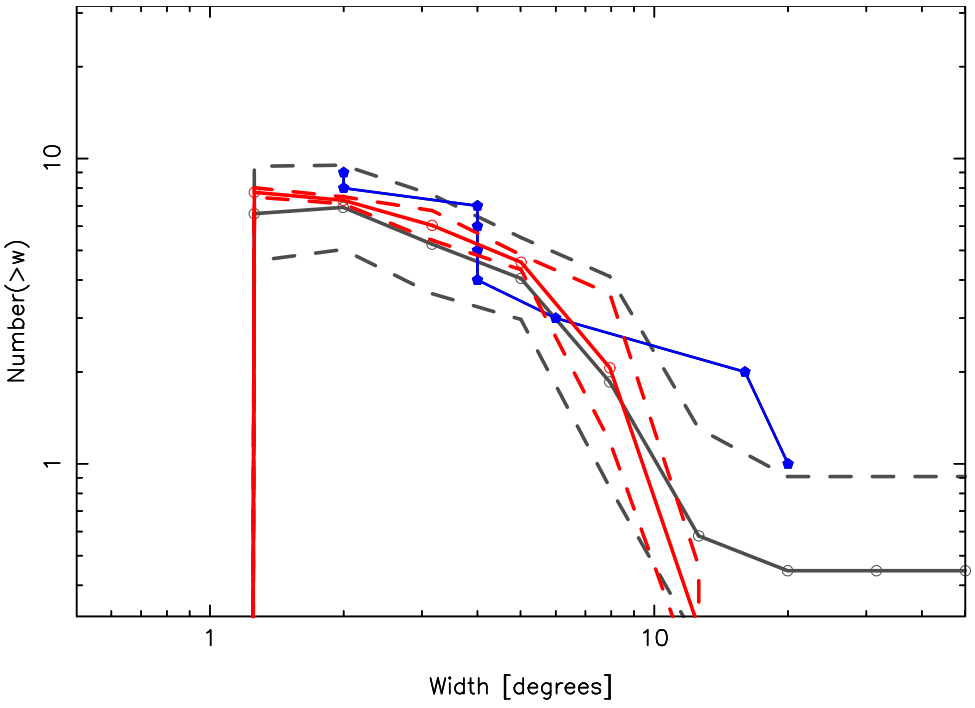


Fig. 9.— Same as Figure 7 but for streams that are pure noise for a 0.1 gap height threshold. Comparison to Figure 7 (top panel, shown in grey here) shows that a real stream has significantly more gaps at 10° and more.

4.3. GD-1 Noise matched Streams

Neither Figure 7 nor Figure 9 have the statistics of the GD-1 stream, where the estimated s/n of a density bin is 2.3. The simulations have a mean s/n per 2° bin of 8.5, having higher numbers of particles than stars in the current data and no foreground noise. To create a stream with statistical properties comparable to GD-1 we first randomly select a subset of the particles from the each simulation used in Figure 7 and then add Gaussian noise to reflect the noise in the foreground/background distribution. There are about 10,000 particles lost from each simulations. Half of those particles are in the leading arm of the stream. Grillmair & Dionatos (2006) estimated the number of stars in their 63° stream segment as 1800 ± 200. We are using the 73° segment from Carlberg & Grillmair (2013) which is longer but probes the same depth in the sky, so estimate that there are about 2500 stars. Therefore the stream data has about half the numbers of stars as particles in the simulation streams. To allow for the noise in the foreground which has been subtracted we add a Gaussian noise that corresponds to a background of 225 units to each density bin. The outcome is that the sub-sampled, noise-added simulation data have a mean signal-to-noise of 2.3, equal to that for GD-1. We then measure the gaps, repeating the sampling and noise addition process 11 times on an individual stream to create an average. The result is displayed in Figure 10. The outcome is close but definitely not identical to the result for a pure noise spectrum since there are more large, 10° and up, gaps than pure noise. However the noise matched stream gap distribution falls somewhat short of what is seen in GD-1 for large gaps. This may be a statistical fluctuation, or, it could point to some systematic error in the data at larger scales. Or, there could be somewhat more large sub-halos that expected in a virialized LCDM galaxy halo. Although the excess of large gaps relative to the LCDM prediction is interesting and could call for an enhanced sub-halo population in the inner halo, we will examine this issue again as better data become available.

5. Discussion and Conclusions

The gap filtering approach is a decomposition of the density along a stellar stream, $d(\phi)$, to a filtered density field $D(\phi, g)$, where g is related to the length of the gap, here $\mathrm{w} \leq 6g$. The filtered distribution is then examined to find the local peaks, after which we find the g value which provides the highest peak at a given ϕ. The outcome is a set of gaps along the stream that are characterized with their width and the minimum height required of the gap. The cumulative distribution of gap sizes, $N(> \mathrm{w})$, is a way of characterizing the density fluctuations in the stream.

To develop insight into this distribution we do identical measurements on a suite of

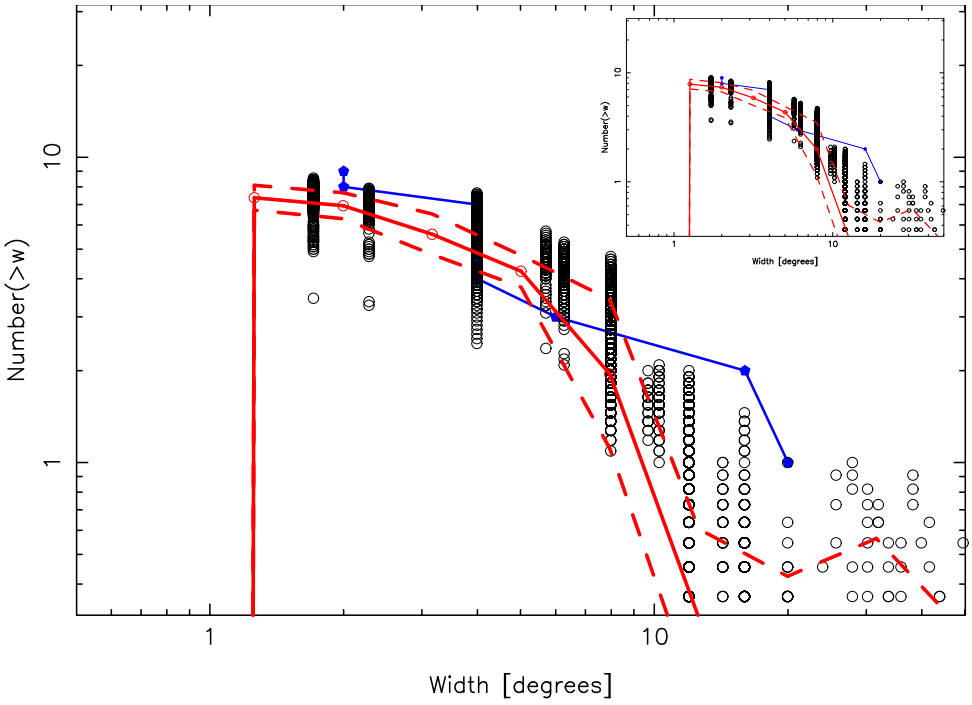


Fig. 10.— Same as Figure 7 but for streams that are randomly sampled to 50% of their density, with noise added to approximate the signal to noise of GD-1. The gap height threshold is 0.1. The inset shows the results with a 0.01 gap height threshold which is essentially identical to the higher threshold version. The circles show the results for each simulation, so the large angle gaps are in excess of the standard sub-halo predictions.

GD-1 like streams that develop in a Milky-Way potential with and without sub-halos. The distribution of gaps sizes stabilizes after about a half dozen orbits, 3 Gyr, so the density variations are not very sensitive to the age of the stream or precisely how much mass is in the sub-halos. In comparison to a stream that is simply a random density field, the GD-1 stream has a significant excess of large gaps. That is, what the filters find to be large gaps are the source of the excess variance in the GD-1 stream above the noise level. However, if the simulations have their signal to noise artificially reduced to the level of the GD-1 stream, the simulations do not produce enough large gaps to match the data, although the discrepancy is not large. One possible explanation is that we have over-estimated the random errors which are added to the simulation data, or, there are unresolved 10 degree scale systematic errors in the measurement of the GD-1 density distribution. Another possibility is that the sub-halo mass distribution has relatively more massive sub-halos in the standard Aquarius halo which we use to normalize our results.

The filters used here are simple first steps, adequate to indicate the nature of the excess variance in GD-1 given the current data. Future data with improved signal to noise for density measurements along the stream will merit a more thorough exploration of filters. In particular, the current data has signal-to-noise of 2.3 in the 2° density bins, which at the same depth will rise to about 6.6 as foreground stars are removed with new astrometric data and ever-improving photometric techniques. Slightly increased depth will then put the signal-to-noise in the regime of our noise-free simulations and increase the confidence of gap finding to their level. A wider range of shapes will allow much better matches to the shapes of the gaps and provide more confident detections. The signal-to-noise of observational data will improve a lot as proper motions help remove foreground stars and deeper images add more stream stars. A future step is to add stream star velocities to the analysis.

This research was supported by CIFAR and NSERC Canada.

REFERENCES

Aihara, H., Allende Prieto, C., An, D., et al. 2011, ApJS, 193, 29

Bovy, J. 2015, ApJS, 216, 29

Carlberg, R. G. 2009, ApJ, 705, L223

Carlberg, R. G. 2012, ApJ, 748, 20

Carlberg, R. G. 2013, ApJ, 775, 90

Carlberg, R. G. 2015, ApJ, 800, 133

Carlberg, R. G. 2015, ApJ, 808, 15

Carlberg, R. G., & Grillmair, C. J. 2013, ApJ, 768, 171

Diemand J., Kuhlen M., Madau P., 2007, ApJ, 667, 859

Erkal, D., & Belokurov, V. 2015, MNRAS, 450, 1136

Grillmair, C. J. 2009, ApJ, 693, 1118

Grillmair, C. J., 2011, ApJ, 738, 98

Grillmair, C. J., & Dionatos, O. 2006, ApJ, 643, L17

Johnston, K. V. 1998, ApJ, 495, 297

Koposov, S. E., Rix, H.-W., & Hogg, D. W. 2010, ApJ, 712, 260

Kroupa, P. 2015, Canadian Journal of Physics, 93, 169

Küpper, A. H. W., MacLeod, A., & Heggie, D. C. 2008, MNRAS, 387, 1248

Küpper, A. H. W., Kroupa, P., Baumgardt, H., & Heggie, D. C. 2010, MNRAS, 401, 105

Küpper, A. H. W., Lane, R. R., & Heggie, D. C. 2012, MNRAS, 420, 2700

Lynden-Bell, D. 1976, MNRAS, 174, 695

Munn, J. A., Monet, D. G., Levine, S. E., et al. 2004, AJ, 127, 3034

Munn, J. A., Monet, D. G., Levine, S. E., et al. 2008, AJ, 136, 895

Navarro, J. F., Frenk, C. S., & White, S. D. M. 1997, ApJ, 490, 493

Ngan, W. H. W., & Carlberg, R. G. 2014, ApJ, 788, 181

Pawlowski, M. S., Pflamm-Altenburg, J., & Kroupa, P. 2012, MNRAS, 423, 1109

Pawlowski, M. S. 2016, MNRAS, 456, 448

Pawlowski, M. S., & Kroupa, P. 2014, ApJ, 790, 74

Price-Whelan, A. M., Johnston, K. V., Valluri, M., et al. 2015, arXiv:1507.08662

Rockosi, C. M., Odenkirchen, M., Grebel, E. K., et al. 2002, AJ, 124, 349

Sanders, J. L., Bovy, J., & Erkal, D. 2015, arXiv:1510.03426

Springel, V. et al. 2008, MNRAS, 391, 1685

Stadel, J., Potter, D., Moore, B., et al. 2009, MNRAS, 398, L21

Willett, B. A., Newberg, H. J., Zhang, H., Yanny, B., & Beers, T. C. 2009, ApJ, 697, 207

Yanny, B., Rockosi, C., Newberg, H. J., et al. 2009, AJ, 137, 4377

Yoon, J. H., Johnston, K. V., & Hogg, D. W. 2011, ApJ, 731, 58

York, D. G., Adelman, J., Anderson, J. E., Jr., et al. 2000, AJ, 120, 1579

This preprint was prepared with the AAS LaTeX macros v5.2.